Supplementary information for:

A miRNA biosensor based on localized surface plasmon resonance enhanced by surface-bound hybridization chain reaction

Andrea Miti, Sophie Thamm, Philipp Muller, Andrea Csàki, Wolfgang Fritzsche, Giampaolo Zuccheri

A. Miti, G. Zuccheri,

Department of Pharmacy and Biotechnology, University of Bologna, Italy

S3 Center, Institute of Nanoscience of the Italian CNR3

Sophie Thamm, Philipp Muller, Andrea Csàki, Wolfgang Fritzsche

Leibniz Institute of Photonic Technology, Albert-Einstein-Str. 9, 07745 Jena, Germany

S1. Extended methods section on LSPR and additional results

S1.1 Reagents and buffers

Reagents and chemicals used during the work were purchased at Merck KGaA (Darmstadt, Germany) and used without any further purification unless specified. All buffers used during this work were prepared in ultrapure water (18 MΩ·cm). Oligonucleotides (Table S1) were purchased at Eurofins Genomics Germany GmbH (Ebersberg, Germany) and biomers.net GmbH (Ulm, Germany). HCR buffer: 0.5 M NaCl, 50 mM NaH_2PO_4, pH 6.8: Citrate Buffer (adsorption buffer): 0.5 M trisodium citrate dihydrate, pH 6.0 (with HCl). Running buffer: HCR buffer 0.75 M NaCl, 75 mM NaH_2PO_4, pH 6.8 (with HCl). 1 mM 6-mercapto-1-hexanol (MCH) in running buffer; HCl 20 mM in ultrapure water. All buffers and solution were additionally filtered with 0.2 µm filters before use. Immobilization buffer: Citrate Buffer 0.5 M pH 6.0. Spherical Gold Nanoparticles 80 nm in diameter (OD_{520} 1, c = 2.89×10^{-4} M, 1.10×10^{10} P/mL) by BBI Solutions (Crumlin, UK).

S1.2 LSPR measurement set-up

The optical LSPR setup was composed of a halogen light source (HL-2000 by Ocean Optics Inc., Dunedin, USA) with a bandpass filter <400 nm, a spectrometer (Flame s UV-VIS by Ocean Optics GmbH, Ostfildern, Germany), and two custom made optical large-core fibers. The microfluidic system involved a computer-controlled peristaltic pump (Ismatec Reglo ICC by Cole-Parmer GmbH, Wertheim, Germany), and a custom-made fluidic cell with tubings (Tygon LMT-55, 0.13 mm inner diameter by Techlab GmbH, Braunschweig, Germany). See also (Thamm et al. 2018) for further details.

S1.3 LSPR Chip preparation

One of the advantages of the method proposed is the simple production of the LSPR chips, employing commercially available spherical 80 nm gold nanoparticles. No specific instrumentation is required; thus, the entire procedure is less expensive compared to the fabrication of flat metallic surfaces for SPR. Such procedure is more convenient for the implementation in biosensing application, thanks to the simple elements required and the high number of chips obtainable in one batch.

The glass slides were carefully cleaned with a rinsing agent (soap) then subjected to multiple sonication: 10 min in Acetone, 10 min in Rotisol (denatured ethanol), 10 min in ethanol and 10 min in ultrapure water.
The glass slides were then dried with nitrogen flow, before plasma etching by oxygen plasma for 60 min, 380 W and 1.6 mbar to remove organic residues and activate them for the subsequent silanization (Oxygen plasma etcher 200G Plasma System by TePla GmbH, Wettenberg, Germany). The affinity between the glass surface and the gold nanoparticles was increased with aminosilanes.
A solution of 1 % APTES in 1 mM acetic acid was prepared and let hydrolyze for 10 min. The cleaned slides were soaked with the APTES solution for 10 min. The slides were then washed in ultrapure water and gently dried with nitrogen flow.

A solution of citrate capped 80 nm gold nanoparticles (BBI Solutions, Cardiff, UK) was centrifuged 8 min at 3220 X g (Centrifuge, UniCen 15DR by Herolab GmbH, Wiesloch, Germany) and 1800 mL of supernatant discarded to get 10-fold concentrated solution of gold nanoparticles. We dropped 20 µL of the concentrated gold nanoparticles solution in the center of the amino-functionalized glass slides and left adsorbing 60 min. The slides were then gently rinsed with ultrapure water and dried with nitrogen flow. At the end of the procedure, a red spot should be visible in the center of the glass. The so prepared chips were stored in closed petri dishes until use.
The density of adsorbed gold nanoparticles depends on the concentration of the colloidal gold and it was optimized under AFM control (see Fig. S1) and checking the spectra of the immobilized gold nanoparticles. The large majority of the inter-particle distances had to be enough to get a sharp plasmon band (see spectra in Fig. 1 in the main text and in Fig. S2 below).
LSPR chips prepared as described above were rinsed with 2 mL of ultrapure water, 2 mL of EtOH and additionally 2 mL of ultrapure water. The thiolated probe was reduced using TCEP 0.5 M. We added to the probe solution in ultrapure water a volume of TCEP 0.5 M to get 20 mM in the final solution and we incubated the mixture at room temperature for at least 1 h. The probe was then diluted to 2 µM in citrate buffer 0.5 M, pH 6.0. The immobilization was performed by layering on the chip 50 µL of this solution and incubating for about 16 hours at room temperature in closed petri dish to avoid evaporation. After the overnight incubation, the glass slides were rinsed with 2 mL of citrate buffer, 2 mL of ultrapure water and stored in the HCR buffer.

In order to evaluate the variability in chips performances, the signal obtained injecting 1 µM of the specific target was compared between different functionalized chips. The mean value of the signal recorded in different sensors was 0.62 ± 0.10 nm, with a %CV of 0.16 %, as evaluated on 5 sensors.

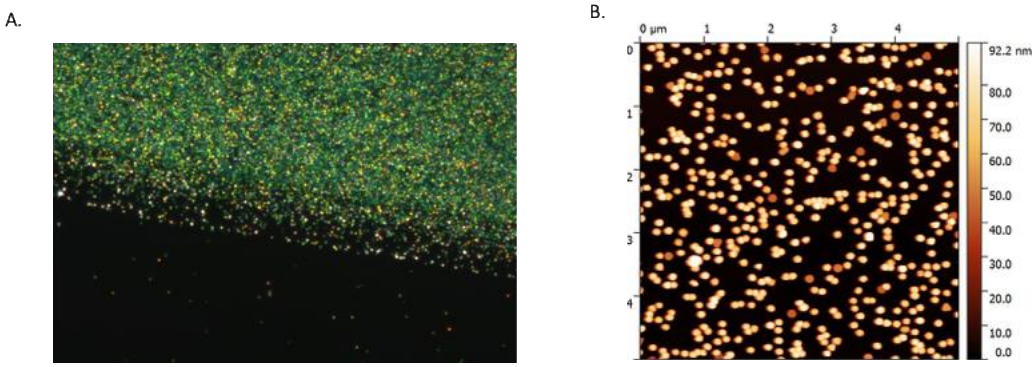

Figure S1. A) Dark field microscopy image showing the immobilized 80 nm gold nanoparticles on the silanized glass substrate. For spherical gold nanoparticles, greenish spots are expected, due to the absorption at about 500 nm and consequently the greenish reflection. This behavior is expected for properly spaced 80 nm gold nanoparticles, while they appear reddish when locally more aggregated. B) AFM micrograph of the same chip.

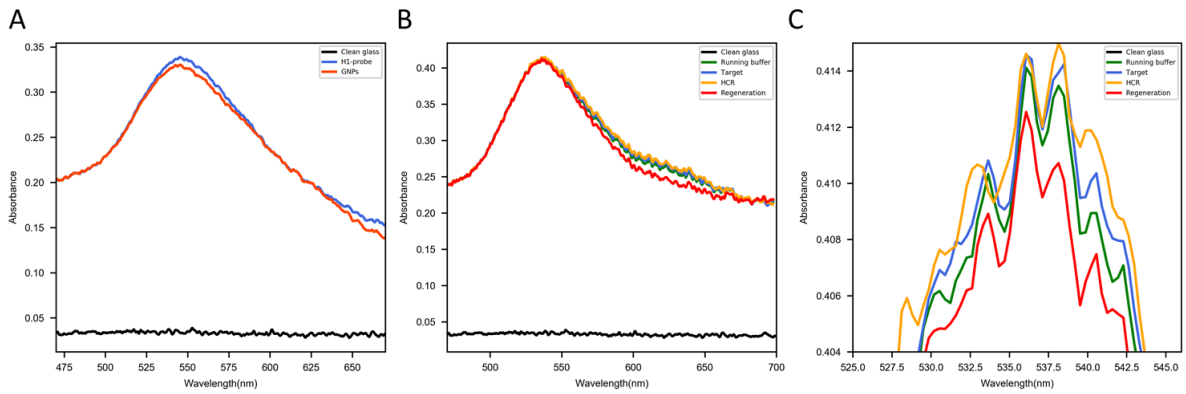

Figure S2. Raw recorded spectra of the LSPR biosensors as prepared and at the different steps in the analytical procedure. A) spectra of an example gold nanoparticle (GNP) chip and of the pristine biosensor with the immobilized hairpin oligonucleotide probe; B) spectra of the different steps in the bioanalytical procedure; C) detain of the peak region for the spectra of panel B. Polynomial fitting was commonly used to smooth the spectra (as shown in the main text Fig. 1).

S1.4 Measurement procedures

A custom-built Python program (Python 3.6) was used to perform the measurements and control the LSPR setup. The chip was inserted in the fluidic chamber in the presence of buffer, in contact with a PDMS gasket. The lamp spectrum was recorded, making sure that no over or under exposure occurred. All the measurements were done in flow conditions, a spectrum was recorded every 2 s. In order to reduce the noise affecting the position of the LSPR peak during the measurement, the centroid of the LSPR peak was calculated at each recorded point according to a previously described method (Dahlin et al. 2006). Oligonucleotides were diluted in running buffer and heated up to 95°C for 5 min, then let cool down at room temperature before use. The measurements were performed in running buffer (see section S1). A solution of 6-mercapto-1-hexanol (MCH, by Merck KGaA, Darmstadt, Germany) 1 mM in running buffer was injected for 300 s at 20 µL/min flowrate. After MCH, the glass surface was incubated with salmon sperm DNA (Deoxyribonucleic acid sodium salt from salmon testes by Merck KGaA, Darmstadt, Germany) at a concentration of 1 mg/mL in running buffer for passivation. Target and hairpins oligonucleotides were flowed at 5 µL/min. The desired concentration of miR-17 oligo was injected for 600 s in the chamber. After the detection step, running buffer was flowed until the signal was stable. To test the hybridization chain reaction, volumes of 1 µM concentrated species of hairpins in running buffer were mixed to get 0.5 µM each and flowed in the chamber for at least 30 min at 5 µL/min. The regeneration of the sensor was obtained with 20 mM solution of HCl, injected for 600 s at 30 µL/min. The general steps and more details are summarized in Table S1.

Steps	flowrate_1	flowrate_2	flowrate_3	flowrate_4	Time (s)	Step
1	20			10	300	HCR buffer
2	5			20	300	**MCH**
3	20			10	400	HCR buffer
4	5			20	300	**Salmon Sperm DNA**
5	20		10		400	HCR buffer
6	2		5		600	**target 1µM**
7	20	10			600	HCR buffer
8	2	5			1000	**HCR**
9	20			10	600	HCR buffer
10	2			30	800	**Regeneration**
11	20		10		400	HCR buffer

Table S1. Description of the protocol used during a typical experiment, with flow rate in µL/min for the channels available, the duration of each step in seconds and the composition of each sample flowed in the chamber in the corresponding step. A pre-flow was used to shorten the transition between the different solutions.

S1.5 Additional data for the detection on LSPR chips

In this section some additional data relative to the sensor performance are showed. Figure S3 shows the response of centroid position when target miR-17 is detected and regeneration performed in order to reuse the LSPR chip. Fig. S4 highlights the difference between unspecific response with miR-106b sequence and the specific one. Only miR-17 induced a fast change in centroid position when flowed in the chamber, while miR-106b at the same concentration (1 µM) induced a weak change. The construction of the calibration curve in Fig. 2 (blue line) in the main text was performed by repeating the detection of the different miR-17 concentration, with multiple regeneration of the sensor. An example of repeated target detection is shown in Fig. S5. Hybridization Chain Reaction was then tested on the sensor. Fig. S6 shows a control experiments performed adding the individual hairpins one by one. It can be estimated that the plasmonic properties of 80 nm gold nanoparticles in these conditions are sensitive to the neighboring solution environment up to a distance of about 40 nm (Jatschka et al., 2016). Consequently, it can be expected that the assembly of only up to 4 or 5 pairs of HCR hairpins could be detected in LSPR and this was verified in our experiments when performing HCR in a step-by-step manner (see Fig. S6). From our previous measurements (Spiga et al., 2014), it could be seen that surface-bound HCR can exceed such assembly lengths. While using LSPR, it is thus not crucial to maximize the HCR assembly yield as this should not lead to a significant improvement of the reported signal amplification factor. On the other hand, this implies that the HCR time could be reduced with respect to other detection strategies, to the advantage of the rapidity of the assay. This was done to prove the working principle of the self-assembly, involving the consecutive binding of the hairpins H1 and H2 in the right order. It Is to note that the injection of H1 as first hairpin does not induce any significant response, compared to the following injection of H2. The result of the consecutive addition of the hairpins is a step by step building process. This is also useful to evaluate the maximum length of the nanostructure we can detect with this technique. The experiment showed in Fig. S7 is a control experiment performed in order to evaluate the unspecific absorption of the hairpin on the surface of the

gold nanoparticles after passivation with MCH, while S8 depicts the change in the centroid position over time occurring when HCR is performed by injecting the mixture of hairpins. Fig. S9 shows the repeated detection of 10 nM miR-17 including the HCR step, as example of data used to construct the curve in Fig. 2 (orange line).

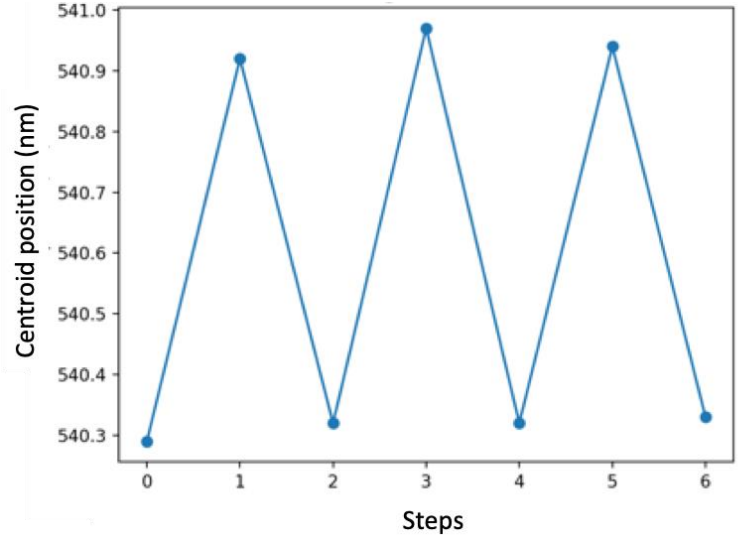

Figure S3. Example of testing the regeneration of the LSPR sensor with HCl 20 mM. HCl 20 mM was selected after trials with different solutions, such as NaOH 0.1 M and Urea 7 M. HCl 20 mM returned the best results in terms of signal recovery after hybridization. The spots correspond to the values of centroid position after each step. Consecutive cycles of hybridization of the target and regeneration through HCl 20 mM were performed.

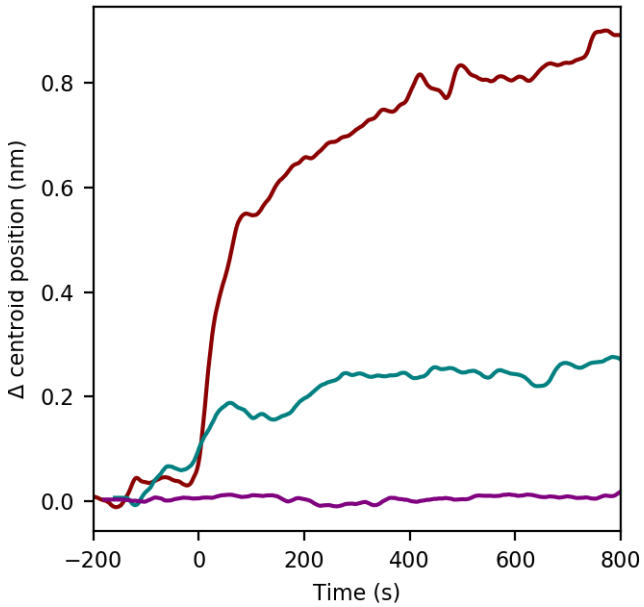

Figure S4. Centroid position over time obtained flowing 1 µM miR-17 sequence (red line), 1 µM miR-106b (green line) and buffer (purple line) in the chamber. The kinetics during the measurements was very different between the two different miRNA sequences. The interaction with miR-17 is very fast and approaches the saturation of the sensor after 800 s, while miR-106b shows a first steep but low interaction then the position of the centroid seems to

shift much slower. Likely, after a much longer time, the shift in the centroid position would be relevant for miR-106b too, but in the timescale of the experiment the system was able to return a significantly different response thus ensuring the specificity.

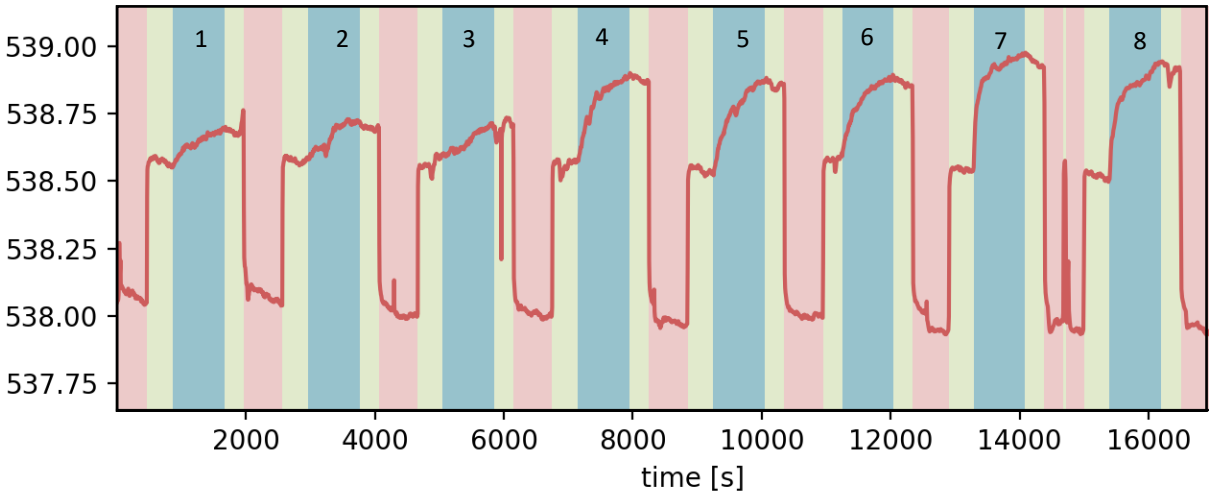

Figure S5: Plot of the centroid position over time with the consecutive injections of different concentrations of the specific target miR-17 (aquamarine) interspersed with regeneration steps (red) and running buffer (light green). Steps 1, 2 and 3 corresponds to 10 nM target injection; steps 4, 5, 6 to 100 nM target; steps 7 and 8 are obtained injecting 1 µM of the specific target.

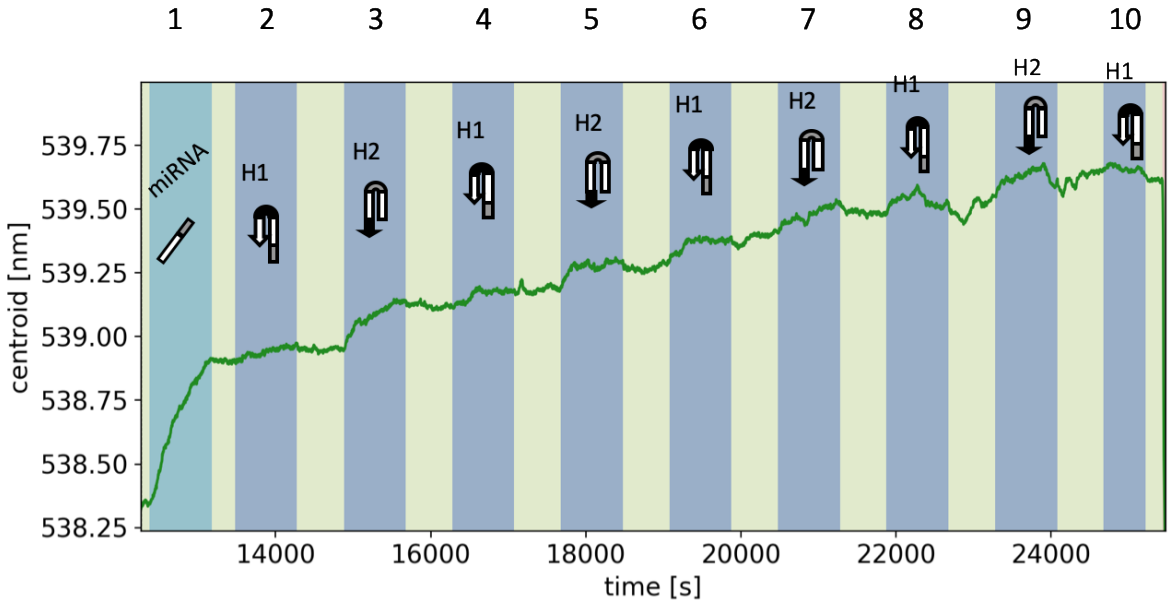

Figure S6: Plot of the centroid position over time with the consecutive addition of the individual hairpins one by one with steps highlighted. Aquamarine corresponds to miR-17 at 1 µM; Blue steps correspond to individual hairpins H1 and H2. Light green is for running buffer. The first injection of hairpin H1 (step 2, at about 14000 seconds), as expected, did not lead to any change on the LSPR peak position, since H1 cannot interact with the probe, which shares the same sequence. On the other hand, H2 could interact with H1 when opened by the target, and led to a change in the peak position. In LSPR, the penetration depth is determined by the diameter of the nanoparticles in use. For spherical nanoparticles, the range is estimated to be

about half of the diameter of the nanoparticle (see also in the main text). For 80 nm gold nanoparticles, the sensitivity region is expected to reach about 40 nm around the nanoparticles. In the B-DNA conformation, the HCR product would reach that length when made of 4 couples of assembled hairpins. Possible deviations from this behavior are expected depending on the packing of DNA around the nanoparticles and on the density of electrostatic charges.

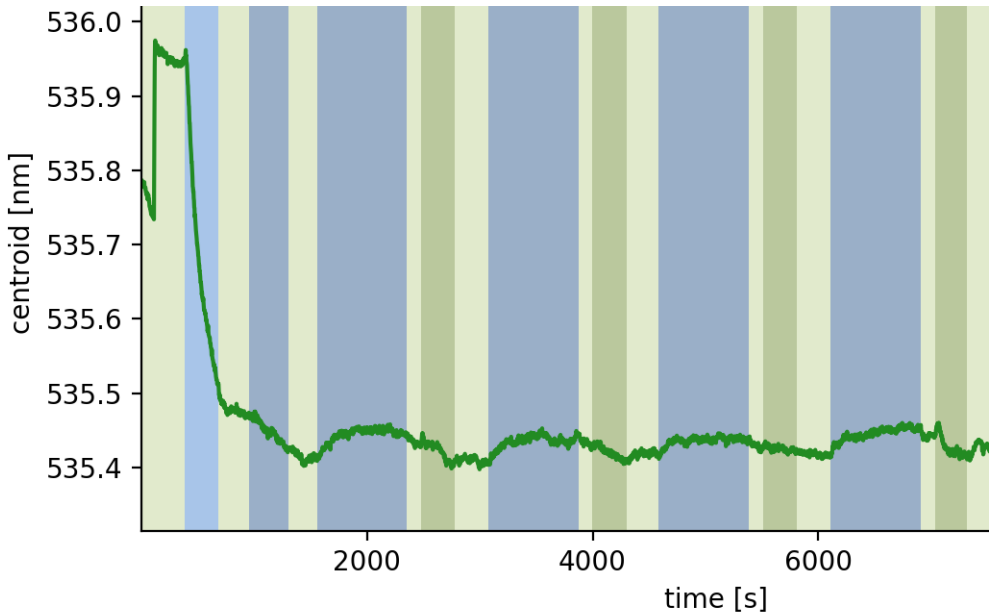

Figure S7. Experiment performed with the aim to evaluate the non-specific absorption of the hairpins on the passivated sensor. We observed a slight shift of the LSPR peak when the mix of hairpins was flowed (blue intervals) rapidly reaching the baseline after flowing running buffer (light green and green intervals). The chips were passivated with 1 mM MCH in running buffer. The first light blue interval corresponds to the MCH step.

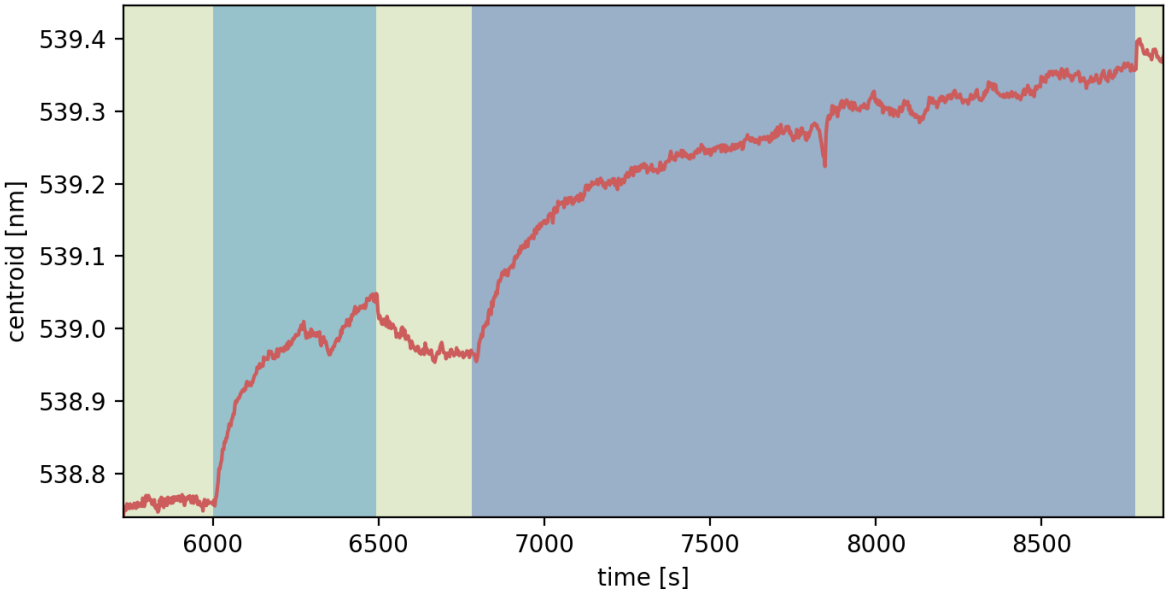

Figure S8. Example of a measurement performed during hybridization chain reaction. The light green intervals correspond to running buffer injections, aquamarine green corresponds to miR-17 injection, while the blue interval corresponds to the injection of the mixture of hairpins.

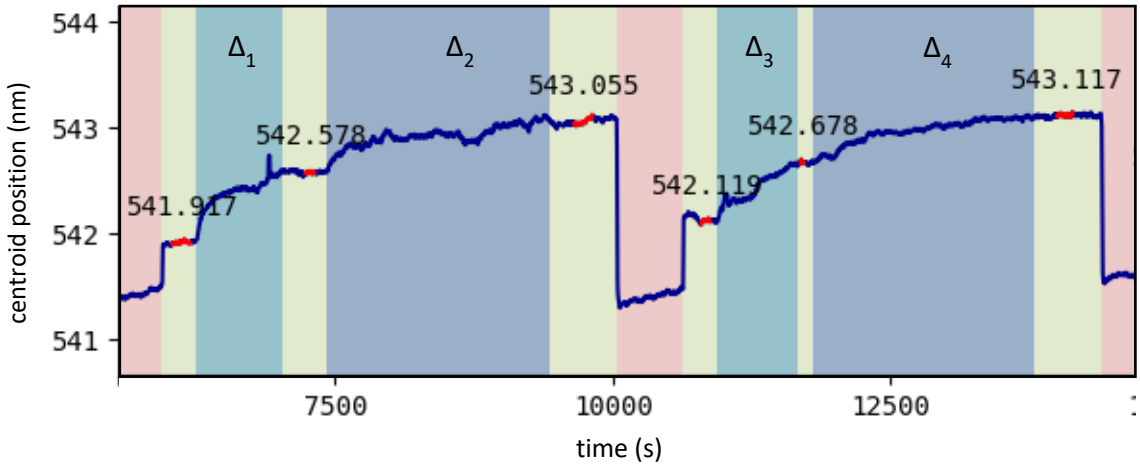

Figure S9. Example of a repeated measurements performed during hybridization chain reaction for 10 nM target concentration. The shifts (Δ) were calculated by taking the difference between the peak position of the plasmonic sensor after and before the injection of miR-17 and hairpins. $\boldsymbol{\lambda_{LSPR}}$ used were the average values of peak position in the red intervals (black numbers in the plot). Δ1 = 0.661 nm, Δ2 = 0.447 nm, Δ3 = 0.559 nm, Δ4 = 0.439 nm. The light green intervals correspond to running buffer injections, aquamarine green corresponds to miR-17 injection, while the blue interval corresponds to the injection of the mixture of hairpins. The data were then normalized on response obtained with 1 µM miR-17 and then used for the construction of the calibration curve.

S2. Review of the recent related bioanalytical methods

In the table S2 below, a literature review highlighting the related bioanalytical procedures available in the scientific literature and known to us. In the remarks column, is a brief summary of the advantages and drawbacks of the literature procedures in order to make a comparison with the one presented in this communication. The review is made to include papers exploiting HCR in a label-free approach.

Label-free biosensing does not require the labeling of the target molecule to perform the detection, since the intrinsic properties of the target such as its size, charge or molecular weight can be exploited. The Hybridization Chain Reaction can be adapted to such approaches in different ways. The DNA nanostructure assembled in the process can be easily labeled in place of the target through additional reagents or by modifying the HCR monomers in order to return an enhanced response (Yang et al 2015, Hou et al 2015, Ding et al 2018). Alternatively, the HCR product can simply further enhance changes in physical properties due to the target recognition. That is the case of methods based on Surface Plasmon Resonance (SPR), electrical impedance, Nanopores based strategies and acoustic detection (Guo et al 2017, Spiga et al 2014, Zhao et al 2017, Cai et al 2017, Xu et al 2019). The procedure we propose in this communication based on Localized Surface Plasmon Resonance has the same advantages as the latter, simple in principle and cost-effective.

Table S2.

Analytical method	Strategy	Target	LOD	Remarks	Reference
Fluorescence	Label-free, SiNPs fluorescence quenching and HCR signal amplification with G-quadruplex	miRNA let-7a	2.5 pM	Does not require enzymes, no laboring procedures, selective. Requires hours (2h hours incubation at 37°C) and several additions of reagents.	Ding et al 2018
SPR	Label-free, non-linear HCR	PML/RARα	0.72 pM	No enzymes involved, good specificity and sensitivity. More complex self-assembly, requires SPR analytical system.	Guo et al 2017
SPR / electrochemical	Label-free, HCR	Pathogen DNA	1 nM (10-100 fmoles) (SPR) 0.1–0.5 µM (Capacitive)	Compatible with miniaturized and multiplexed parallel sensing. Low sensitivity, SPR intrumentation required.	Spiga et al 2014
Colorimetric	Label-free, AuNps in solution	Short DNA target	50 pM (spectroscopic) 100 pM (visual)	Simple in procedures and relatevely quick (1 h). Not applied to a real target sequence.	Liu et al 2013
Electrochemical	Label-free, nanopore membrane utilizing HCR	Survivin mRNA	30 fM	Good sensitivity. Several hours required	Zhao et al 2017
Electrochemical	Label-free MetB, ITO surface	miRNA let-7a	1 pM	Simple, enzyme-free, immobilization of the probe is not required. Requires incubation at 37°C	Hou et al 2015
Electrochemical	Label-free, DNA hydrogel combining HCR and DNAzyme.assisted recycling	Hg^{2+}	0.042 pM	Sensitive, evaluation of Hg^{2+} in real samples Requires DNAzyme recycle step and hydrogel polymerization	Cai et al 2017

Analytical method	Strategy	Target	LOD	Remarks	Reference
Electrochemical	Label-free, AgNCs	miR-199a	0.64 fM	High sensitivity, good selectivity TAPNR amplification, AgNCs synthesis required during the detection	Yang et al 2015
Acoustic detection	Branched HCR in solution	DNA	25 nM	No enzymes or thermal cycles required Low sensitivity	Xu et al 2019
SPR	Multiple signal amplification through HCR and AuNps	miR-21	0.6 fM	Enzyme-free, sensitive and specific, coupled with magnetic separation Many steps required	Liu et al. 2017
SPR	Multiple signal amplification through HCR and AuNps	miR-21	8 fM	Enzyme-free, sensitive and specific Many steps required	Wang et al. 2016
Localized Surface Plasmon Resonance	Linear HCR on immobilized gold nanoparticles	miR-17	1 pM	Enzyme-free, no thermal cycles, easy production of the chips, relatively quick (1h) Method can be optimized	This work

S3. Oligonucleotide sequences and thermodynamic analysis of their structures

The oligonucleotides used during this work were designed using NUPACK. The thermodynamic analysis of the selected sequences (table S3) was performed in order to evaluate the secondary structures of the individual strands and the interaction between the different strands. Some of the results of the thermodynamic analysis are presented in Fig. S10, S11 and S12.

Strand	Sequence (5' > 3')	nt
miR-17	CAAAGTGCTTACAGTGCAGGTAA	23
miR-106b	TAAAGTGCTGACAGTGCAGAT --	21
miR-21	TAGCTTATCAGACTGATGTTGA	22
H1	CTACCTGCACTGTAAGCACTTTGAATTCGCAAAGTGCTTACAGTGC	46
H2	CAAAGTGCTTACAGTGCAGGTAGGCACTGTAAGCACTTTGCGAATT	46
H1_probe	SH(CH)6-TTTTCTACCTGCACTGTAAGCACTTTGAATTCGCAAAGTGCTTACAGTGC	50

Table S3. Sequences of the oligonucleotides.

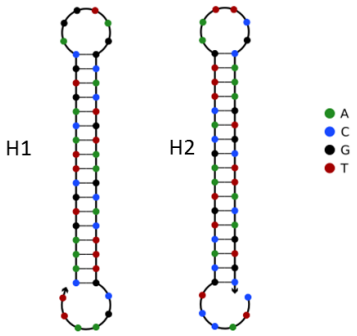

Figure S10. Hairpins H1 and H2 used as monomers of the Hybridization Chain Reaction specific for miR-17

A.

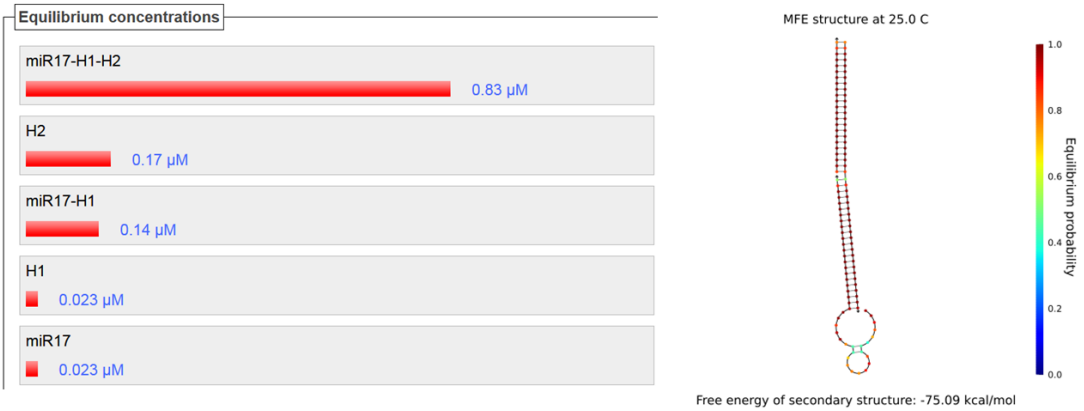

B.

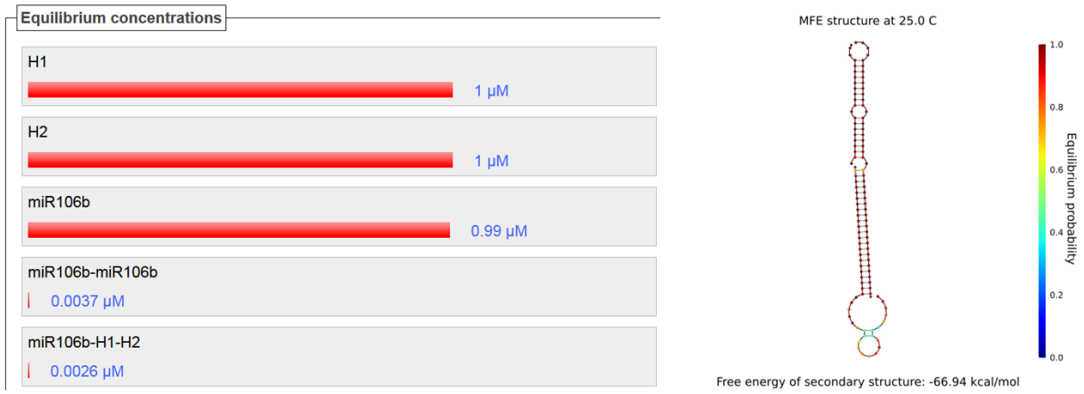

Figure S11. NUPACK analysis of the interaction of H1 and H2 with miR-17 and miR-106b sequences. Here we focused on the first complex involving the three species H1, H2 and miRNA. This would be the first complex triggering required for the nanostructure to grow. A) Analysis of the mixture miR-17 + H1 + H2, 1:1:1, 1 µM concentration. The barplot shows the theoretical concentration of each species at the equilibrium. The formation of the complex miR-17-H1-H2 is favored in these conditions suggesting the correct behavior in triggering the self-assembly. This complex is the preponderant with a ΔG of -75.09 kcal/mol. The figure on the right depicts the minimum free energy structure of the complex, with the base pairing probability in color scale. B) Analysis of the formation of miR-106b-H1-H2. The probability of formation for such complex is much lower. The species are almost not involved in any interaction based on the thermodynamic evaluation returned by NUPACK. The small fraction of complex miR-106b-H1-H2 formed shows a ΔG less favorable compared to the interaction with miR-17, -66.94. NUPACK analysis suggests thus a high capability of discrimination between miR-17 and miR-106b. This is also due to the stability of the interaction between H1 and miR-106b that is considered very improbable by the analysis tool (see also Fig S3).

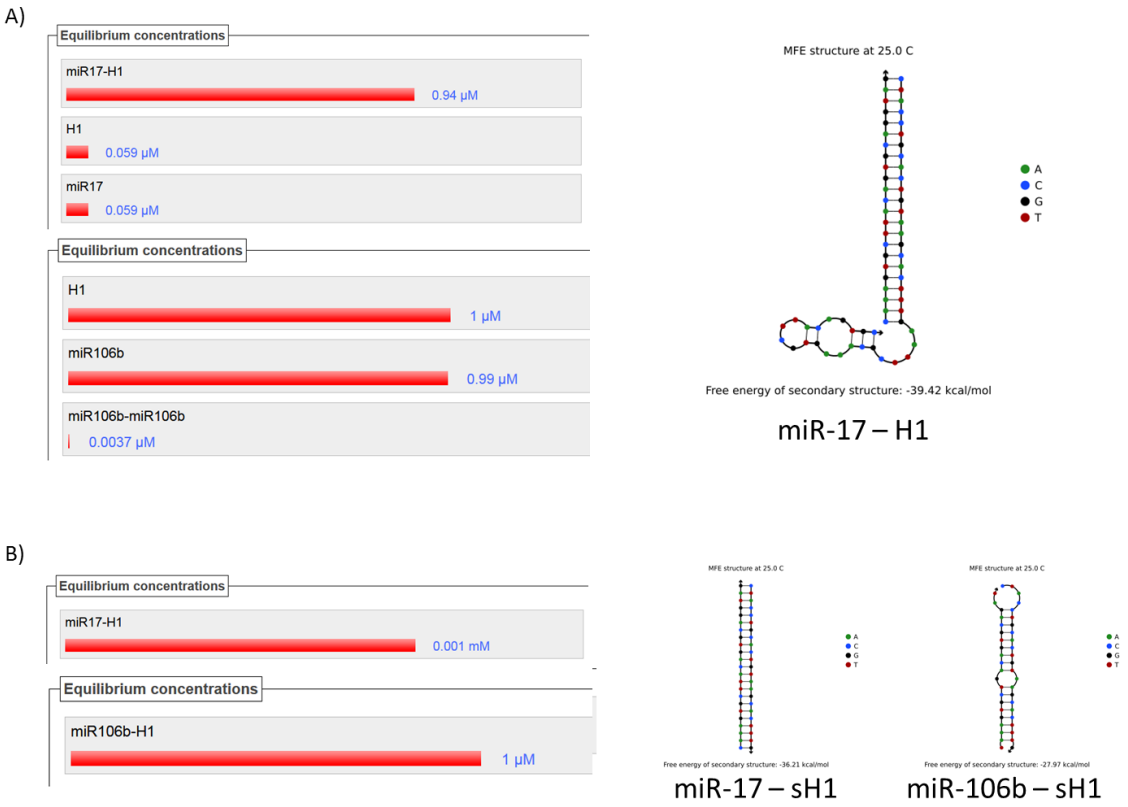

Figure S12. NUPAK thermodynamic analysis of the interaction of H1 with miR-17 ad miR-106b sequences. A) Interaction between miR-17 and H1. The formation of miR-17-H1 complex is favored in the selected conditions leading to the structure showed on the right. As we can observe in the histogram, the interaction with miR-106b does not result in any complex involving the two species, predicted thus to stay in the individual form in solution. This suggests a high specificity in the interaction. B) We tried to perform the same analysis introducing an open sequence of H1. In this configuration, the differences in the sequence of miR-106b are not enough to impede the interaction with sH1 (single stranded H1). This result suggests the advantage of using a hairpin-like probe to enhance the specificity.

S4. Preliminary and additional experiments of HCR in solution

DNA oligonucleotides stock solutions (100 μM) of targets and hairpins were diluted in PCR tubes in HCR buffer in general at 3-times the final concentration. Samples are then subjected to thermal treatment using a thermocycler (Thermo Scientific, PCR Sprint thermal cycler): 95°C for 5 min and allowed to cool down to 20°C in 1 h (0.02°C/sec). The proper volumes of solutions containing H1 and H2 hairpins were mixed, then a volume of target solution was added to the mixture. The reaction was incubated at least for 1 h at room temperature, unless specified. Electrophoresis gel analysis was performed through polyacrylamide gel electrophoresis in TBE 1X buffer: 89 mM Tris–boric acid, pH 8.0, 2 mM ethylenediaminetetraacetic acid tetrasodium salt (EDTA-Na_4). Polyacrylamide gels were prepared at 10% acrylamide in TBE 1X buffer (Acrylamide 40% acrylamide Acrylamide/bis-acrylamide, suitable for electrophoresis, 37.5:1). SYBR Gold (Nucleic Acid Gel Stain, Invitrogen) was then used to visualize the results using a Gel doc (Bio-Rad Gel doc 1000 System). AFM analysis of the HCR products obtained in solution were performed after a purification step. Samples were diluted 1/100 in TE 1X buffer (10 mM Tris-HCl, 1 mM EDTA pH 8.0) and filtered with centrifugal filter units, MWCO 100 kDa (Amicon Ultra-0.5 mL centrifugal filters). The samples were then collected in HEPES buffer (10 mM NaCl, 5 mM $MgCl_2$ pH 7.5). A 10 μL aliquot was spread on a freshly-cleaved muscovite mica disc and left to adsorb for 5 min. The mica surface was then rinsed with ultrapure water and gently dried with nitrogen. Imaging for atomic force microscopy has been carried out using Multimode 8 NanoScope AFM in ScanAsyst Peakforce Tapping™ mode (Bruker).

The formation of the HCR product was characterized in solution through gel electrophoresis analysis and AFM characterization of the DNA nanostructures (Fig. S13 A, B, C and D). Fig. S6 A shows the formation of the DNA nanostructures in presence of the specific target, while Fig. S6 B highlight the different sizes of the HCR product depending on the concentration of the target, a feature of such self-assembly reaction. AFM imaging (Fig. S13 C and D) showed DNA nanostructures with and average size of 200 nm, including nanostructures reaching more than 1 μm.

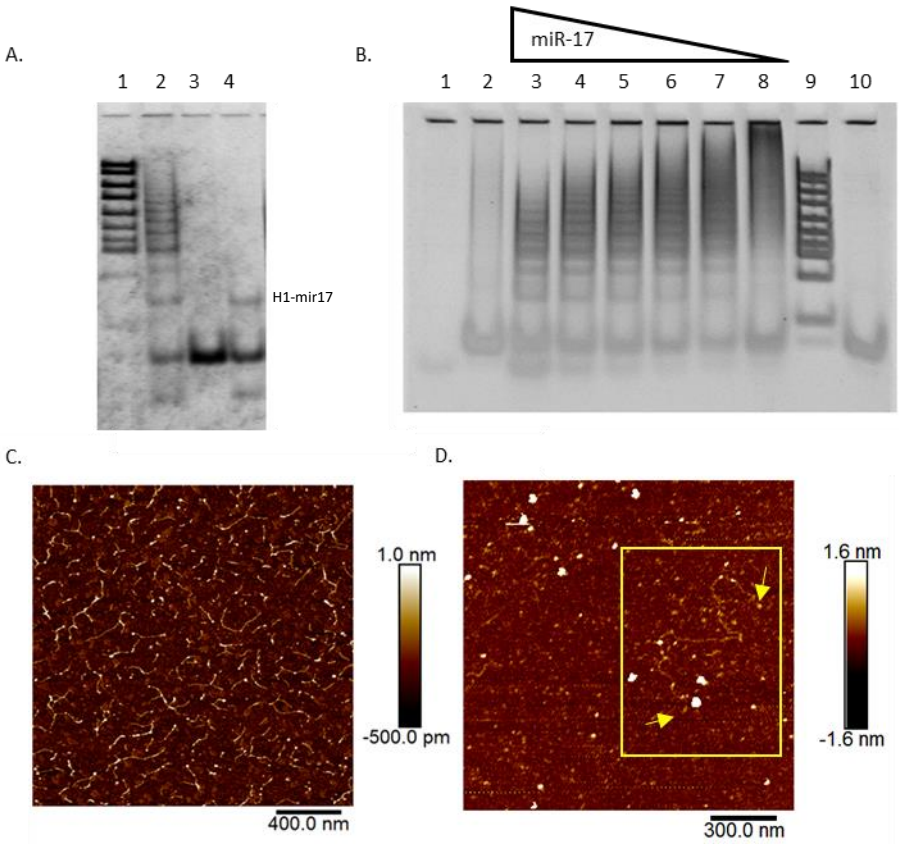

Figure S13: A) Gel electrophoresis showing HCR product (lane 2), the hairpins without target (lane 3) and the mixture H1 + miR-17 (lane 4). Lane 1: molecular weight DNA ladder. B) Section of gel electrophoresis showing the effect of target concentration on the HCR. Lane 1: miR-17; lane 2: hairpins H1 + H2; lane 3-8: miR-17 10 µM, 3 µM, 2 µM, 1 µM, 0.5 µM, 0.1 µM, with 1 µM hairpins concentration. Lane 9: molecular weight DNA ladder; lane 10: H1. C) and D) Atomic force microscopy images showing the HCR products obtained in solution.

S4.1 Testing HCR specificity in solution

The specificity of the reaction in solution was tested by mixing the pair of hairpins with miR-106b sequence. In Fig. S14 it is clear that no product is assembled in presence of the miR-106b sequence, while the reaction is efficiently triggered by miR-17 sequence. The interaction with additional miRNA sequences was also evaluated, as depicted in Fig. S15.
Additional experiments were performed in order to evaluate the rate of the self-assembly, the effect of temperature and the effect of BSA in solution, to test the versatility and the suitability in conditions closer to biosensing applications (Fig. S16 and S17).

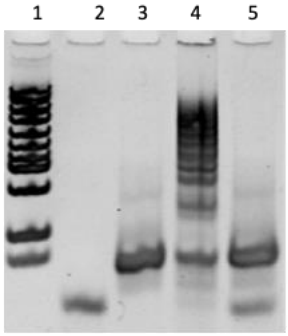

Figure S14: Polyacrylamide gel electrophoresis showing HCR performed with miR-17 and miR-106b, to compare the specificity. Equimolar conditions 1 µM. Lane2, mir-17; lane 3, H1 and H2; lane 4, full mir-17 HCR; lane 5, failed HCR with 1 µM mir-106b.

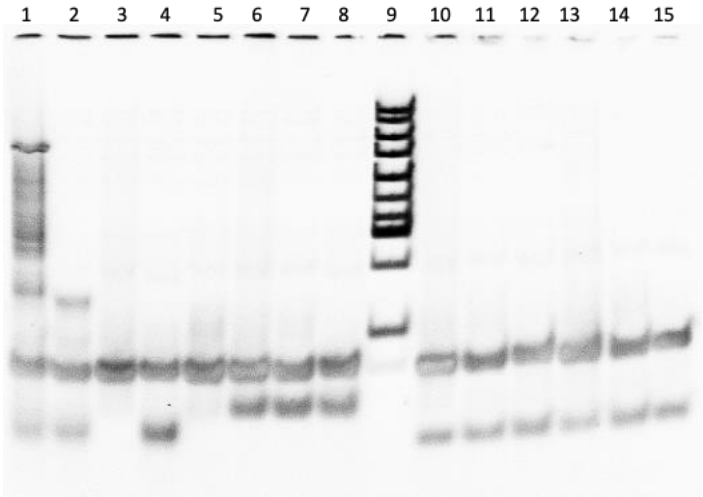

Figure S15. Additional assay of the specificity of mir-17 HCR in solution. Polyacrylamide gel electrophoresis analysis of the effect of non-specific unrelated sequences miR-30c, miR-140-5p and miR-486 in the presence of the mixture of hairpins. This was done to test the stability of the hairpins over sequences not related to the specific target miR-17. Lane 1: H1 + H2 + miR-17; lane 2: H1 + miR-17; lane 3: H1 + H2. Lane 4: H2 + miR-17; lane 5: H2; lane 6: H1 + H2 + miR-30c; lane 7: H1 + miR-30c; lane 8: H2 + miR-30c; lane 10: H1 + H2 + miR-140-5p; lane 11: H1 + miR-140-5p; lane 12: H2 + miR-140-5p; lane 13: H1 + H2 + miR-486; lane 14: H1 + miR-486; lane 15: H2 + miR-486.

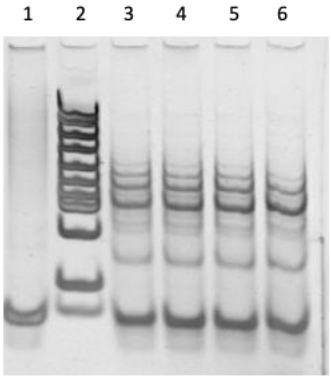

Figure S16. Polyacrylamide gel electrophoresis analysis of the reaction product at different incubations times. Different hybridization chain reactions were started at different times before the electrophoretic analysis. HCR product at different incubation time within 2h. Lane 1: H1 + H2; lane 2: DNA ladder molecular weight marker; HCR products at lane 3 and higher: lane 3, 15 min; lane 4: 30 min; lane 5: 1 h; lane 6; 2 h.

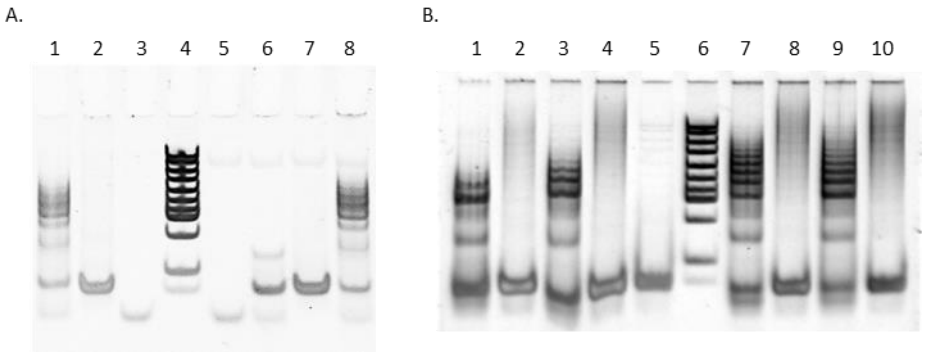

Figure S17. A) Demonstration that HCR can also work in complex matrices. Polyacrylamide gel electrophoresis of the HCR product obtained in HCR buffer and in presence of 12.5 % (bovine serum albumin) BSA in HCR buffer to simulate the complex matrix of the blood serum. Lane 1: full HCR with mir-17; lane 2: H1 + H2; lane 3: miR-17; lane 4: DNA ladder molecular weight marker; lane 5: miR-17 in HCR buffer with 12.5 % BSA; H1 + miR-17 in HCR buffer with 12.5 % BSA; lane 7: H1 + H2 in HCR buffer with 12.5% BSA; lane 8: HCR in HCR buffer with 12.5 % BSA. B) Proof of the robustness of the designed HCR at different temperatures. Lane 1: HCR at 15 °C; lane 2: H1 + H2 at 15 °C; lane 3: HCR at 25 °C; lane 4: H1 + H2 at 25 °C; lane 5: H1 + H2; lane 6: DNA ladder molecular weight marker; lane 7: HCR at 35 °C; lane 8: H1 + H2 at 35 °C; lane 9: HCR at 45 °C; lane 10: H1 + H2 at 45 °C.

References

Cai, W., Xie, S.B., Zhang, J., Tang, D.Y., Tang, Y., 2017 Biosensors & Bioelectronics 98, 466-472.

Dahlin, A.B., Tegenfeldt, J.O., Hook, F., 2006 Analytical Chemistry 78(13), 4416-4423.

Ding, L.H., Liu, H.Y., Zhang, L.N., Li, L., Yu, J.H., 2018 Sensors and Actuators B-Chemical 254, 370-376.

Guo, B., Cheng, W., Xu, Y.J., Zhou, X.Y., Li, X.M., Ding, X.J., Ding, S.J., 2017 Scientific Reports 7.

Hou, T., Li, W., Liu, X.J., Li, F., 2015 Analytical Chemistry 87(22), 11368-11374.

Jatschka, J., Dathe, A., Csáki, A., Fritzsche, W., Stranik, O., 2016. Sensing and Bio-Sensing Research 7, 62-70.

Liu, P., Yang, X.H., Sun, S., Wang, Q., Wang, K.M., Huang, J., Liu, J.B., He, L.L., 2013 Analytical Chemistry 85(16), 7689-7695.

Liu, R.J., Wang, Q., Li, Q., Yang, X.H., Wang, K.M., Nie, W.Y., 2017 Biosensors & Bioelectronics 87, 433-438.

Spiga, F.M., Bonyar, A., Ring, B., Onofri, M., Vinelli, A., Santha, H., Guiducci, C., Zuccheri, G., 2014 Biosensors & Bioelectronics 54, 102-108.

Thamm, S., Csàki, A., Fritzsche, W., 2018. LSPR Detection of Nucleic Acids on Nanoparticle Monolayers, in: Zuccheri, G. (Ed.), DNA Nanotechnology: Methods and Protocols. Springer New York, New York, NY, pp. 163 - 171.

Xu, G.L., Lai, M.L., Wilson, R., Glidle, A., Reboud, J., Cooper, J.M., 2019. Microsystems & Nanoengineering 5.

Wang, Q., Liu, R.J., Yang, X.H., Wang, K.M., Zhu, J.Q., He, L.L., Li, Q., 2016. Sensors and Actuators B-Chemical 223, 613-620.

Yang, C.Y., Shi, K., Dou, B.T., Xiang, Y., Chai, Y.Q., Yuan, R., 2015. ACS Applied Materials & Interfaces 7(2), 1188-1193.

Zhao, T., Zhang, H.S., Tang, H., Jiang, J.H., 2017 Talanta 175, 121-126.